

FINAL
02-0236

Paper AAS 02-164



**Using Inertial Measurements for the
Reconstruction Of 6-DOF
Entry, Descent, and Landing Trajectory and
Attitude Profiles**

Geoffrey G. Wawrzyniak and Michael E. Lisano

**Jet Propulsion Laboratory, California Institute of
Technology**

San Antonio, Texas

27-30 January 2002

AAS Publications Office, P.O. Box 28130, San Diego, CA 92198

Mechanics Meeting

USING INERTIAL MEASUREMENTS FOR THE RECONSTRUCTION OF 6-DOF ENTRY, DESCENT, AND LANDING TRAJECTORY AND ATTITUDE PROFILES

Geoffrey G. Wawrzyniak and Michael E. Lisano

A method was sought for estimating the “stroke” distance between a Mars Exploration Rover (MER) test lander (protected by airbags) and a surface during impact. The authors at JPL have developed a suite of software known as REDLand (for Reconstruction of Entry, Descent and Landing) to accomplish this. REDLand uses data from accelerometers and gyroscopes on board the lander test body as measurements in an extended Kalman filter, in addition to geometric and dynamical constraints, and other data, where available. This paper is a discussion of the formulation of the REDLand filter algorithms and presents results from actual MER airbag-and-lander impact tests made in 2001.

INTRODUCTION

In 2003, humans on the planet Earth will launch two spacecraft towards the planet Mars. The Mars Exploration Rovers (MER-A and MER-B) are scheduled to land on the surface of the Mars weeks apart in early 2004. They can travel nearly as far in a day as the Mars Pathfinder (MPF) Sojourner rover did in its lifetime. The MER missions have heritage in the MPF mission in that each will enter the atmosphere on a ballistic trajectory, deploy a parachute while traveling at supersonic speeds, and use airbags to survive the impact on the surface of the planet. Understanding MER-A’s entry, descent, and landing (EDL) is critical to the success of its twin’s EDL twenty-one days later.

Currently, tests of the MER landers’ airbag systems are underway, and data collected during these tests are being used at the Jet Propulsion Laboratory (JPL) to develop and test a prototype extended Kalman filter (EKF) for EDL.

The airbag tests are being conducted at the Space Power Facility (SPF) vacuum chamber at NASA’s Glenn Research Center Plum Brook Station in Sandusky, Ohio. During these tests, the SPF is evacuated to simulate the approximately five-torr atmosphere near the Martian surface. A mock-up of the MER lander body is suspended above a rocky inclined plane and, with airbags inflated, it is tethered to the ground with a stretched bungee cable. To initiate a test, the line holding the lander is cut and the bungee cable acts with gravity to accelerate the lander towards the plane. The resulting impact simulates an impact scenario on the surface of Mars. From this test, the impact robustness of the airbags can be evaluated and the loads from the shock of impact can be determined.

The lander body is outfitted with a suite of instruments, some of which are used in automotive crash tests. Accelerometers and gyroscopes measure translational and rotational data, which can be used in an EKF to reconstruct the trajectory and attitude history of the lander during the drop test. No direct measurements of distance traveled by the test body, or its speed or attitude, are available.

One testing objective, which motivates the work discussed here, is to determine the “maximum stroke” distance during the impact event to within ten centimeters (3σ). Maximum stroke is the shortest distance between the airbag surface and the tetrahedron-shaped lander body. A full stroke event would occur if the airbags compressed to the point where the rigid body of the lander would no longer be protected from hitting the surface, potentially damaging the lander body and the instrumentation contained within. The maximum stroke distance is a function of airbag test parameters, especially airbag pressure and impact velocity, both of which can be controlled in order to avoid a full-stroke event. The maximum stroke distance is not easily measured, however, because the airbags themselves fully obscure viewing of the lander with a camera or laser device, for example. Hence, an indirect method of sensing maximum stroke distance based on accelerometer and gyroscope data, in addition to geometric and dynamical constraints and other sensed information “as available,” was sought.

The authors have developed a suite of software in the Java (TM) Programming Language known as REDLand (for Reconstruction of Entry, Descent and Landing), which uses the accelerometer and gyroscope rate data, as well as other data as available, as measurements in the filter. This represents a departure from the standard practice of simply integrating the noisy acceleration and body rate measurements to determine distance traveled, speed, and attitude. In this case, the accelerations due to the bungee and gravity are modeled in the EKF equations of motion, and the accelerometer and gyroscope measurements are used to adjust dynamics model parameters.

MER EDL SEQUENCE

The MER airbags are integral to the MER atmospheric entry, descent and landing strategy, which closely follows the “parachute-retrorocket-airbag” paradigm established by the MPF mission.

In this Pathfinder-like EDL strategy, each MER lander, enclosed in an aerodynamic capsule with a forward-facing heat shield and an aft-facing back shell, enters the Martian atmosphere at speeds greater than five kilometers-per-second. The capsules decelerate from hypersonic speeds in the upper atmosphere, experiencing a peak deceleration around six Earth G's. Parachute deployment occurs at about eight kilometers altitude, while still traveling at supersonic speed. Twenty seconds after parachute deployment, the heat shield is ejected. Ten seconds later, the tetrahedron-shaped lander body separates from the back shell of the aerodynamic capsule, and is lowered down a Kevlar line, or bridle, that is suspended from the inside of the back shell. This “EDL stack,” consisting of the parachute, back shell, and lander body suspended on the bridle, continues to descend, and the radar onboard the lander is activated. Sixteen seconds later, when the lander is a few hundred meters over the ground, a set of airbags is inflated on all sides of the lander body. Two seconds later, a cluster of retrorockets in the back shell is ignited, firing for approximately four seconds to decelerate the vertical speed of the lander body with respect to the ground to zero velocity. An instant later, a mechanism at the top of the lander body severs the bridle, and the lander body, surrounded by airbags, drops the final ten to twenty meters to the surface, impacting the ground at speeds of up to twenty meters-per-second.

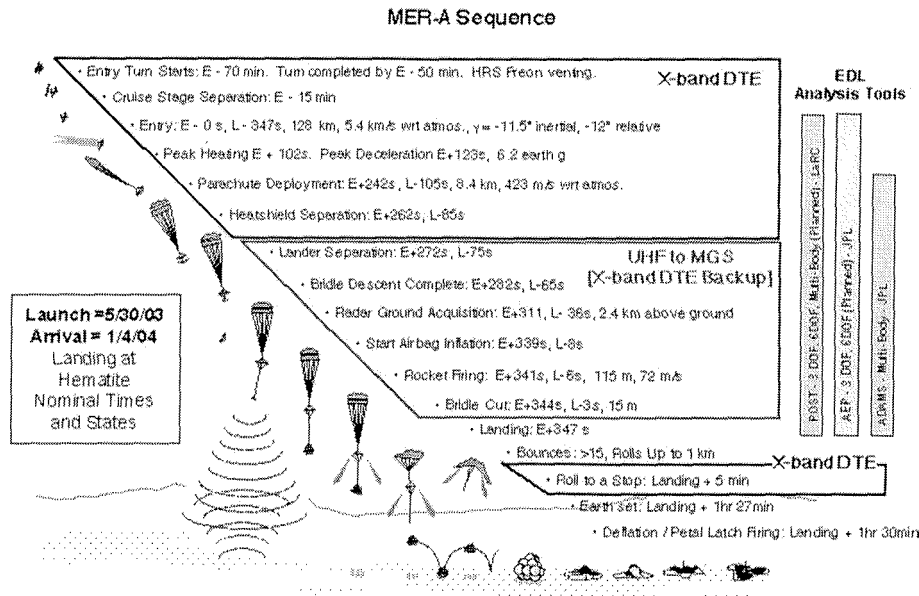


Figure 1: Illustration of MER-A's EDL to the Hematite candidate landing site (*illustration courtesy of Phil Knocke*).

It is expected, based on Mars Pathfinder experience, that the MER lander body, protected by its airbags, could bounce more than fifteen times, and travel a horizontal distance of as much as a kilometer, before coming to a stop. The sequence ends, finally, when the airbags are deflated and retracted, and the lander body petals open to release the Mars Exploration Rover robots to begin scientific observation of the Martian surface. Figure 1 is an illustration of MER-A'S EDL to the Hematite candidate landing site.

TEST ARTICLE AND EQUIPMENT

While cushioning the impact of a MER flight lander on Mars with airbags is a concept from the Mars Pathfinder mission of 1997, the geometry and mass of the MER lander and its payload (the rover) are different than the MPF lander. The shapes of each mission's landers are identical and tetrahedral, but the size and mass of a MER lander is slightly larger. Like the MPF lander, the MER lander has a central base petal with three hinged side petals that open for rover egress. The primary purpose of the drop tests discussed in this paper is to characterize the MER airbag landing system. Therefore, the MER test lander need only to be similar to the MER flight lander in geometry and mass (materials and inertial properties differ between the two landers).

The MER drop test lander is essentially an aluminum cage with a data acquisition system to record airbag pressures, lander kinematics, and loads during a drop test. When

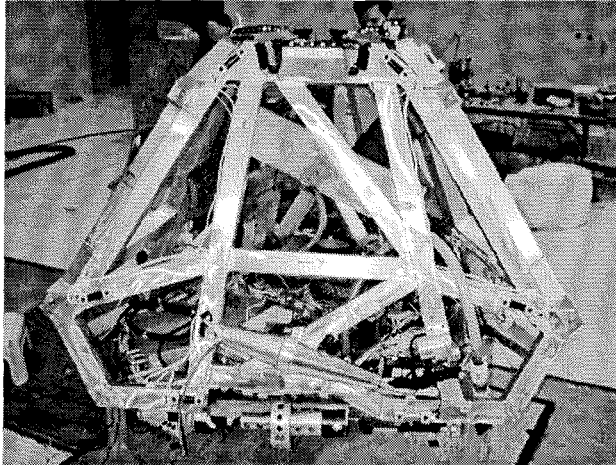


Figure 2: The MER airbag drop test lander is fully instrumented and awaits attachment of the airbags (*photo courtesy of ILC Dover, Inc.*).

closed, the lander is 1.2 meters tall and each side is 1.6 meters at the base. The lander frame was constructed so that an instrument panel (home to the data acquisition system and many of its transducers) could be easily mounted and removed from inner side of the base petal. Additionally, ballast mass can be added to each of the side petals. The frame of the lander is made entirely of 6061-T6 welded aluminum. Figure 2 is a picture of the test lander with the petals in closed position.

The MER airbags are manufactured by ILC Dover, Inc., the same company that developed and manufactured the MPF airbags. Each airbag has six, two meter diameter lobes arranged in a “billiard rack” design. The three side airbags vent into the base airbag, and vice versa, to prevent any one airbag from bursting due to pressure on impact. Figure 3 shows the airbags inflated during a post-drop inspection. The airbags are made of a Vectran HS base fabric. The material chosen for the airbags needed to be lightweight, have high tensile and tear strengths, operate flexibly in environmental extremes, leak resistant, and have a low coefficient of friction.² The drop tests also allow for experimentation of four different configurations of weave and layering (each bag is different in this respect). The four configurations for the drop series discussed in this paper are four layers of 200 denier (alternating pattern), five layers of 100 denier, two internal layers of 100 denier and two external layers of 200 denier, and four layers of 200 denier (normal pattern). Finally, a bladder is inside each airbag, which is made of the same Vectran airbag material, but has a silicon coating to provide gas retention.

Testing is conducted in a near vacuum condition, and the lander can experience harsh impact conditions. A data acquisition system must be able to operate in these conditions. The Intelligent Dummy Data Acquisition System (IDDAS) from SoMat Corporation and Robert A. Denton Inc. is a data acquisition system that was designed for automotive crash tests. It was used in MPF testing and again in MER testing. The IDDAS can run on batteries, collect up to 260 thousand epochs of data on a maximum of 48 channels (depend-

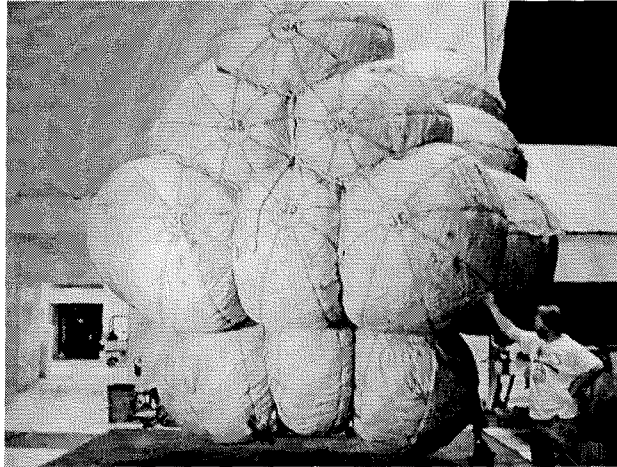


Figure 3: The MER airbag drop test lander in the preparation room near the SPF. Each rock on the ramp is colored with chalk, which leaves a distinct indication of which rocks were hit by the airbags during the drop test (*photo courtesy of ILC Dover, Inc.*).

ing on the IDDAS model), collect samples at a maximum rate of 19230 samples-per-second, and withstand high acceleration environments and extreme environmental conditions. The IDDAS filtering rate is 500 Hz. During a drop test, the IDDAS begins collecting data a few seconds before release and collects data throughout the drop and post-drop settling period. The data is held in memory until it can be off-loaded by the test engineer after the lander is retrieved from the re-pressurized chamber.

Data types from a number of different transducers have been collected during previous drops: bag and ambient pressures and temperatures, airbag tendon loads, latch-pin loads, airbag displacement, rotation rates, and accelerations. The transducers connected to the IDDAS must be of a bridge circuit or ± 5.0 volt excitation. This paper is primarily concerned with the data from the rate gyroscopes and accelerometers. It should be noted that measurements of airbag displacements were made using string and infrared potentiometers, however, both of these techniques can only determine the location of a point on the bag with respect to lander. String and infrared potentiometers are two ways to measure stroke directly, but neither can give the full picture like a trajectory reconstruction.

The triaxial rate gyroscope, CFX Technologies Model UG11384A, can measure ± 1000 degrees-per-second and can withstand a shock of 200 G over one millisecond. Their accuracy is specified by the manufacturer to be ± 3 percent. The accelerometers are ENDEVCO Model 7264B Piezoresistive Accelerometers. To measure accelerations in three-dimensional space, three accelerometers are mounted to a mounting block (ENDEVCO Model 7964A), which has dimensions of 16.51 by 16.51 by 10.92 mm³ (see Figure 4). Designed for anthropomorphic dummy instrumentation, the accelerometers have a range of ± 2000 G. The damping ratio of an accelerometer is 0.005 and the resonance frequency is 28000 Hz. Their accuracy is approximately 0.2 G. For each test, four triads of accelerometers were placed on the instrument panel as shown in Figure 5. Future tests will incorporate

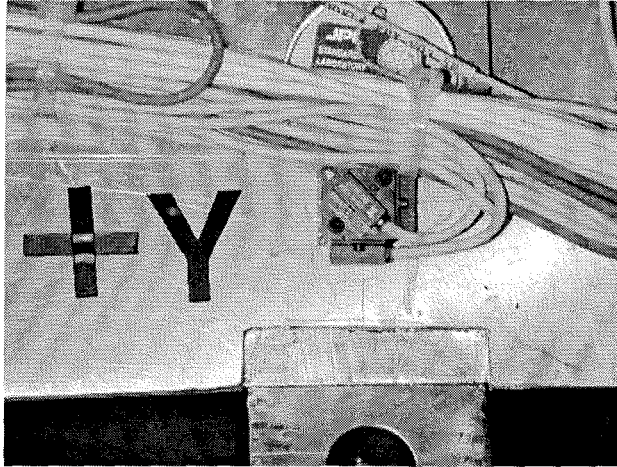


Figure 4: Three ENDEVCO model accelerometers (blue) mounted orthogonally on a block (red). This accelerometer is located on the positive Y edge of the base petal, or PYBP (*photo courtesy of ILC Dover, Inc.*).

accelerometers on the tops of the side petals.

Finally, an instrument was selected to provide data for the determination of initial attitude. As described in Wertz,⁸ two non-parallel vectors can be used to form a direction-cosine matrix. Each test plan calls for an initial orientation based on which bag is the “down-bag” or “up-bag” (the face normal that is directed towards or away from the ground, respectively) and which is the “trailing bag” or “leading bag” (the face normal that is directed towards or away from the ramp direction, respectively). For a rough approximation of initial orientation, these face normals can be used. For a better approximation of initial orientation, an instrument that can sense gravity and Earth’s magnetic field is employed. The MicroStrain 3DM uses a triaxial accelerometer set and a triaxial magnetometer set to report the directions of gravity and Earth’s magnetic field. The 3DM can report roll-pitch-yaw angles or raw bits of the two triaxial sets of sensor. For these tests, biases and gains were found from a calibration routine, then used to convert the raw bits data into gravity and magnetic field unit vectors. These unit vectors were then used in the “Algebraic Method” for determination of the rotation matrix found in Wertz. This rotation matrix was then converted into a quaternion.

TEST FACILITY

While the MER landers are different enough from the MPF lander, the concept of using of airbags to cushion the lander during impact with the Martian surface is one of the more apparent segments of the MER missions to have heritage in the Mars Pathfinder mission. In 1995 and 1996, a series of drop tests were performed at the Space Power Facility (SPF) at NASA Glenn Research Center’s Plum Brook Station, in Sandusky, Ohio, to validate airbags as a landing technique.⁷ Fortunately, many of the MPF era elements of

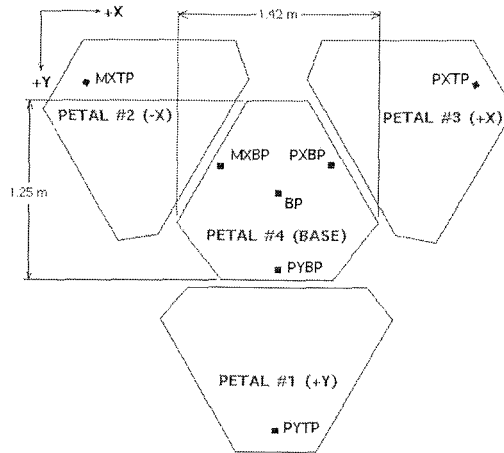


Figure 5: Diagram of lander coordinate system and possible accelerometer mounting locations on an opened lander. Each location is named according to a direction based convention (e.g., PYBP is the plus Y base petal, MXTP is the minus X top petal, etc.).

the SPF are still available for use on MER. The SPF is again being used for purposes of airbag verification — this time for the MER missions.

The SPF is considered the “world’s largest space environment simulation chamber”.⁶ The inner diameter of the test chamber is 30.5 meters, and the floor to ceiling measures 37.2 meters. The inner aluminum chamber is surrounded by an concrete outer pressure vessel. Figure 6 is a drawing of the SPF outlining its main features. The SPF can be pumped down to 10^{-6} torr and simulate space temperature and radiation. For purposes of these tests, the chamber needs only to be pumped down to approximately 5 torr, or one Martian atmosphere.

One of the most obvious hold-overs from the MPF tests is a 60 degree inclined plane with a rock field used to simulated a Martian surface impact of 30 degrees. This ramp is approximately 15.5 meters tall and has a rock field on its face. The rock field is not fixed and is often reconfigured between tests. Lava rocks from 0.2 meters to 0.5 meters have been used to test the airbags’ resistance to ripping. Rocks are spaced approximately one meter apart to subject the airbag to “bridging,” where the airbag stretches and forms a bridge between the rocks on impact. The incline of the plane is used to test what is believe to be a 3σ worst-case scenario at impact on Mars, where the lander has a horizontal velocity of approximately sixteen meters-per-second and a vertical velocity of approximately twelve meters-per-second. The horizontal velocity may be due to high wind conditions. The vertical velocity at impact is due to a bridle-release drop from fifteen meters above the Martian surface. A nominal impact would have a minimal horizontal velocity.

In order to meet the required impact speeds, a bungee tow-rope system is used with gravity to accelerate the lander towards the ramp. The spring force on the bungee system

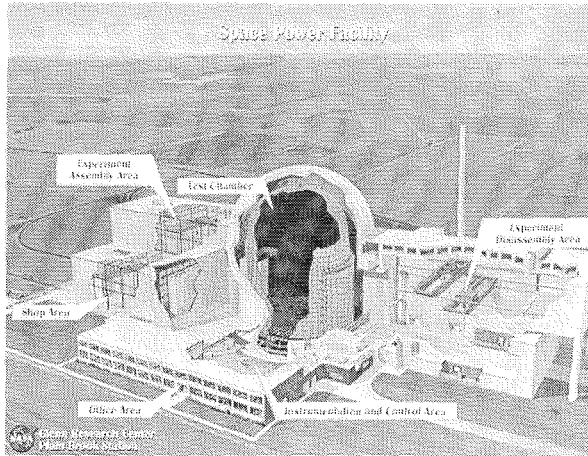


Figure 6: Illustration of the Space Power Facility in Sandusky, Ohio.⁶

as a function of stretch distance, Δx , and number of bungees, N , can be accurately modeled with a third or fourth order polynomial. Before each test, the test engineer calculates the number of bungees and bungee stretch distance required to accelerate the lander to its final velocity based on the energy equation

$$\frac{1}{2}mv_{impact}^2 - mg_0h = \int_{x_0}^{x_0+\Delta x} f(x, N)dx, \quad (1)$$

where m is the mass of the lander/airbag system plus the acceleration system and the drop height, h , is dependent on the stretch distance, Δx .

After the initial release of the lander, the bungee pulls the lander towards the ramp until a hammer (which is on the line that connects the lander to the bungee system) hits a nail that triggers a pyro to release the bungee system from the lander. This nail is located approximately 0.3 meters below the center of the ramp and 7.3 meters above the ground. The nail is the origin of the SPF reference frame. The Z-axis is pointed up, the Y-axis is towards the face of the ramp, and the X-axis cross product of Y and Z. A -60 degree rotation about the SPF X-axis is required to visualize results in a “Mars” frame.

TYPICAL TEST SEQUENCE

The airbag development model test have been conducted in three series at present. The first two series of drop tests utilized the MPF drop test lander. The third series employed the MER drop test lander. One more development model series will be conducted in January and February of this year, followed by engineering and qualification test series over the next year and a half. The setup and executions sequences are generally the same for each drop test. This section describes those sequences.⁵

Setup for the for the first drop test in a series begins weeks in advance. The chamber must be readied for the series by installing the ramp in the chamber, installing the rock

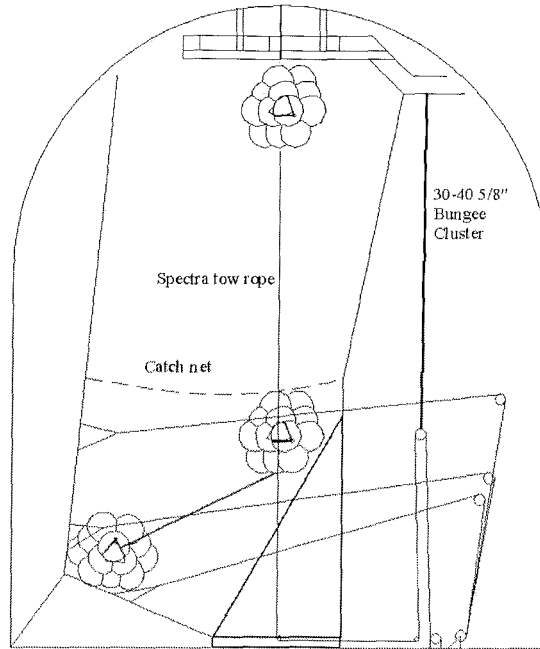


Figure 7: Diagram of the test article set-up in the SPF's main chamber. After the lander is released, it accelerates towards and bounces off the ramp and into a catch net (*drawing courtesy of Tom Rivellini*).

field on the ramp, and rigging the bungee acceleration system. High-speed, cinematic, and standard VHS cameras and lighting are installed around the chamber to record the drop. Days before the test, the instrumentation (IDDAS, transducers, etc.) and ballast mass are installed in the lander. The lander is weighed and the center of mass is found. The airbags are then attached to the lander. The day before the drop test, the lander is transported from the assembly area, the bungee line is attached, and an umbilical line from the control room is attached to the lander. The umbilical is the only path of communication between the control room and the instrumentation in the lander. The lander is then raised into position and final end-to-end checks are made. Figure 7 is an drawing of the test article set-up in the SPF.

On the day of the test, the chamber doors are closed, and the chamber is pumped down to five torr. The pump down process takes four to six hours to remove nearly 23 thousand cubic meters of air in the chamber. At this time, the airbags are steadily inflated to the desired bag pressure (1.0 - 1.3 psi). Leak checks on the bag are conducted throughout the inflation process. The bungees are then set to the preload required for the desired impact velocity. Approximately five to ten seconds before the drop, the IDDAS begins recording data from the transducers and the cameras are turned on.

To commence the drop, a command is sent from the control room to fire a pyro on the release rope, which suspends the lander from the ceiling of the chamber. The release rope is cut and the bungee system and gravity are now unopposed and the lander is pulled towards

the ramp. Immediately after the release, the umbilical separates at its slip connection. Just before the airbags contact the ramp, a hammer on the impact rope hits a nail located just under the ramp. The nail triggers a microswitch that sends a command to fire a pyro that severs the impact rope between the hammer and the lander. The bag is now in free fall for about 0.05 seconds. The airbags encounter the ramp and begin to compress. Since all four of the airbags are connected with ducts, air from the “down” bag is forced to other airbags. The pressures in these bags stretch the tendons that suspend the lander inside of the airbags, much like the spokes on a bicycle wheel. The airbags compress and then bounce off of the ramp into a safety net (see Figure 7). If the pressure within the airbags is optimal, then the airbags have no major damage *and* the lander does not contact the ramp, or go “full stroke” — the test is successful. The entire sequence described in this paragraph — from release to the safety net — takes less than 2.5 seconds.

After the drop, the chamber is dived (the chamber is unplugged and air freely refills vacuum). Refilling the chamber takes approximately six to eight hours. Once the pressure in the chamber is equal to the ambient pressure, the lander is removed, the airbags are inspected and the data from the IDDAS is downloaded. Drop tests in a series occur two days apart, as a goal.

ALGORITHM

The equations of motion that are propagated in the REDLand filter can be either dynamic or kinematic in nature. In the dynamic mode, the acceleration of the body due to the bungee is expressed explicitly. In the kinematic mode, no explicit modeling of forces (except gravity) acting on the airbag/lander body is done in the filter. Instead, the measurements from the inertial sensors on the lander body are employed to estimate the non-gravitational accelerations in the filter. This section examines the algorithm used in the REDLand filter.

The acceleration $\tilde{\mathbf{r}}_{\mathbf{o}}$ of center of mass of the airbag/lander body is

$$\tilde{\mathbf{r}}_{\mathbf{o}} = \tilde{\mathbf{f}}_{\text{ng}_o} + \tilde{\mathbf{g}}, \quad (2)$$

where $\tilde{\mathbf{f}}_{\text{ng}_o}$ is the acceleration due to nongravitational forces acting on the body and $\tilde{\mathbf{g}}$ is gravitational acceleration. The acceleration $\tilde{\mathbf{r}}_{\mathbf{a}}$ of a point occupied by an accelerometer, located on the lander body at location $\mathbf{r}_{\mathbf{a}}$ relative to the center of mass, is related to the mass-center acceleration by

$$\tilde{\mathbf{r}}_{\mathbf{a}} = \tilde{\mathbf{r}}_{\mathbf{o}} + \alpha \times \mathbf{r}_{\mathbf{a}} + \omega \times \omega \times \mathbf{r}_{\mathbf{a}}, \quad (3)$$

where α is the angular acceleration of the lander body and ω is its angular rate. This can be expressed in an alternative manner:

$$\tilde{\mathbf{r}}_{\mathbf{a}} = \tilde{\mathbf{r}}_{\mathbf{o}} + [\mathbf{A} + \mathbf{W}]\mathbf{r}_{\mathbf{a}}, \quad (4)$$

where

$$\mathbf{A} = \begin{bmatrix} 0 & -\alpha_z & \alpha_y \\ \alpha_z & 0 & -\alpha_x \\ -\alpha_y & \alpha_x & 0 \end{bmatrix} \quad (5)$$

and

$$\mathbf{W} = \begin{bmatrix} -(\omega_y^2 + \omega_z^2) & \omega_x\omega_y & \omega_x\omega_z \\ \omega_x\omega_y & -(\omega_x^2 + \omega_z^2) & \omega_y\omega_z \\ \omega_x\omega_z & \omega_y\omega_z & -(\omega_x^2 + \omega_y^2) \end{bmatrix}. \quad (6)$$

Now, because the accelerometers are strapped-down, that is, connected to the body as opposed to being gimballed, the attitude of the body must be estimated as well in order to resolve the inertial components of acceleration. Moreover, the accelerometer does not sense gravitational acceleration, so the measured acceleration \mathbf{a}_a is related to the total acceleration $\ddot{\mathbf{r}}_a$ by

$$\mathbf{a}_a = \ddot{\mathbf{r}}_a - \mathbf{g}. \quad (7)$$

In addition to the attitude, the angular rate and acceleration must also be estimated. This is done so that the inertial non-gravitational acceleration may be separated from non-inertial accelerations due to body rotation sensed by the accelerometer. Thus, given the sensed acceleration \mathbf{a}_a , the location \mathbf{r}_a of the accelerometer relative to the lander center of mass, and estimates of ω and α , the inertial non-gravitational accelerations are extracted from the accelerometer measurements using

$$\begin{bmatrix} a_{a/x} \\ a_{a/y} \\ a_{a/z} \end{bmatrix} = \begin{bmatrix} f_{ng_{ox}} \\ f_{ng_{oy}} \\ f_{ng_{oz}} \end{bmatrix} + \begin{bmatrix} -(\omega_y^2 + \omega_z^2) & \omega_x\omega_y - \alpha_z & \omega_x\omega_z + \alpha_y \\ \omega_x\omega_y + \alpha_z & -(\omega_x^2 + \omega_z^2) & \omega_y\omega_z - \alpha_x \\ \omega_x\omega_z - \alpha_y & \omega_y\omega_z + \alpha_x & -(\omega_x^2 + \omega_y^2) \end{bmatrix} \cdot \begin{bmatrix} r_{a/x} \\ r_{a/y} \\ r_{a/z} \end{bmatrix} \quad (8)$$

Given the above equations, a nineteen member state vector \mathbf{X} for the REDLand filter was defined as

$$\mathbf{X} = [\tilde{\mathbf{r}}_o \quad \tilde{\dot{\mathbf{r}}}_o \quad \mathbf{f}_{ng_o} \quad \mathbf{q} \quad \omega \quad \alpha] \quad (9)$$

and its time derivative, yielding the filter equations of motion, is

$$\dot{\mathbf{X}} = [\tilde{\dot{\mathbf{r}}}_o \quad \tilde{\ddot{\mathbf{r}}}_o \quad \dot{\mathbf{f}}_{ng_o} \quad \dot{\mathbf{q}}(\omega) \quad \alpha \quad \dot{\alpha}]. \quad (10)$$

The subscript ‘‘o’’ indicates that the given quantity relates to a reference point, in this case, the center of mass of the lander body. The tildes indicate that the quantity is expressed in some set of inertial coordinates, which are obtained by lander-body-fixed coordinates using

$$\tilde{\mathbf{r}}_o = \mathbf{T}_B^I \ddot{\mathbf{r}}_o, \quad (11)$$

where

$$\mathbf{T}_B^I = \begin{bmatrix} q_1^2 + q_2^2 - q_3^2 - q_4^2 & 2(q_2q_3 + q_1q_4) & 2(q_2q_4 - q_1q_3) \\ 2(q_2q_3 - q_1q_4) & q_1^2 - q_2^2 + q_3^2 - q_4^2 & 2(q_3q_4 + q_1q_2) \\ 2(q_2q_4 + q_1q_3) & 2(q_3q_4 - q_1q_2) & q_1^2 - q_2^2 - q_3^2 + q_4^2 \end{bmatrix}. \quad (12)$$

For this particular problem, it was convenient to work in a quasi-inertial coordinate frame related to the SPF acuum chamber. The Z direction is chosen opposite the direction of

gravity (“up”), X was chosen to be perpendicular to both gravity and a unit vector normal to the ramp face, and Y was chosen to complete the right-handed orthonormal basis.

Next, it is shown that each member of $\dot{\mathbf{X}}$ can be expressed as a function of members of state vector \mathbf{X} . Clearly, $\tilde{\mathbf{r}}_o$ is equal to the velocity members in the state vector. The acceleration $\ddot{\mathbf{r}}_o$ is computed as

$$\ddot{x}_o = \tilde{f}_{ng_{ox}} \quad (13)$$

$$\ddot{y}_o = \tilde{f}_{ng_{oy}} \quad (14)$$

$$\ddot{z}_o = \tilde{f}_{ng_{oz}} - \tilde{g}, \quad (15)$$

where, again, the Z component has been chosen as the direction opposite to gravity.

As attitude is expressed using a quaternion, the time rate of change of attitude must be expressed in terms of the quaternion derivative $\dot{\mathbf{q}}$. This is done with the familiar formula:

$$\dot{\mathbf{q}} = \frac{d\mathbf{q}}{dt} = \frac{1}{2}\Omega\mathbf{q}, \quad (16)$$

where

$$\Omega = \begin{bmatrix} 0 & -\omega_x & -\omega_y & -\omega_z \\ \omega_x & 0 & \omega_z & -\omega_y \\ \omega_y & -\omega_z & 0 & \omega_x \\ \omega_z & \omega_y & -\omega_x & 0 \end{bmatrix}. \quad (17)$$

The derivative α is equal to the angular acceleration members of the state vector. Finally, the time rate of change of the acceleration terms is not generally known *a priori*. However, given a sufficiently high measurement sample rate, $\dot{\mathbf{f}}_{ng_o}$ and α can be treated as time-correlated random variables. This is done by setting $\dot{\mathbf{f}}_{ng_o}$ and $\dot{\alpha}$ to zero. Alternatively, if an *a priori* acceleration model is known, $\dot{\mathbf{f}}_{ng_o}$ can be expressed as an equation.

The filter covariance is propagated from a prior time to the current time using the state transition matrix $\Phi_{19 \times 19}$, which is found to be

$$\Phi_{19 \times 19} = \begin{bmatrix} \mathbf{I}_{3 \times 3} & \Delta t \cdot \mathbf{I}_{3 \times 3} & \frac{\Delta t^2}{2} \cdot \mathbf{T}_{B,3 \times 3}^I & \frac{\Delta t^2}{2} \cdot \Gamma_{3 \times 4} & \mathbf{0}_{3 \times 3} & \mathbf{0}_{3 \times 3} \\ \mathbf{0}_{3 \times 3} & \mathbf{I}_{3 \times 3} & \Delta t \cdot \mathbf{T}_{B,3 \times 3}^I & \Delta t \cdot \Gamma_{3 \times 4} & \mathbf{0}_{3 \times 3} & \mathbf{0}_{3 \times 3} \\ \mathbf{0}_{3 \times 3} & \mathbf{0}_{3 \times 3} & \mathbf{I}_{3 \times 3} & \mathbf{0}_{3 \times 4} & \mathbf{0}_{3 \times 3} & \mathbf{0}_{3 \times 3} \\ \mathbf{0}_{4 \times 3} & \mathbf{0}_{4 \times 3} & \mathbf{0}_{4 \times 3} & \mathbf{I}_{4 \times 4} & \Delta t \cdot \Psi_{4 \times 3} & \mathbf{0}_{4 \times 3} \\ \mathbf{0}_{3 \times 3} & \mathbf{0}_{3 \times 3} & \mathbf{0}_{3 \times 3} & \mathbf{0}_{3 \times 4} & \mathbf{I}_{3 \times 3} & \Delta t \cdot \mathbf{I}_{3 \times 3} \\ \mathbf{0}_{3 \times 3} & \mathbf{0}_{3 \times 3} & \mathbf{0}_{3 \times 3} & \mathbf{0}_{3 \times 4} & \mathbf{0}_{3 \times 3} & \mathbf{I}_{3 \times 3} \end{bmatrix}. \quad (18)$$

The matrix Γ is used to relate the current-time inertial position and velocity to the *a priori*

time attitude quaternion; it is found to be

$$\begin{aligned} \Gamma &= \frac{\partial(\mathbf{T}_B^I \tilde{\mathbf{f}}_{ng_o})}{\partial \mathbf{q}} \\ &= 2 \begin{bmatrix} q_1 \tilde{f}_{ng_{ox}} + q_4 \tilde{f}_{ng_{oy}} - q_3 \tilde{f}_{ng_{oz}} & q_2 \tilde{f}_{ng_{ox}} + q_3 \tilde{f}_{ng_{oy}} + q_4 \tilde{f}_{ng_{oz}} & & \\ -q_4 \tilde{f}_{ng_{ox}} + q_1 \tilde{f}_{ng_{oy}} + q_2 \tilde{f}_{ng_{oz}} & q_3 \tilde{f}_{ng_{ox}} - q_2 \tilde{f}_{ng_{oy}} + q_1 \tilde{f}_{ng_{oz}} & \dots & \\ q_3 \tilde{f}_{ng_{ox}} - q_2 \tilde{f}_{ng_{oy}} + q_1 \tilde{f}_{ng_{oz}} & q_4 \tilde{f}_{ng_{ox}} - q_1 \tilde{f}_{ng_{oy}} - q_2 \tilde{f}_{ng_{oz}} & & \\ & -q_3 \tilde{f}_{ng_{ox}} + q_2 \tilde{f}_{ng_{oy}} - q_1 \tilde{f}_{ng_{oz}} & -q_4 \tilde{f}_{ng_{ox}} + q_1 \tilde{f}_{ng_{oy}} - q_2 \tilde{f}_{ng_{oz}} & \\ \dots & q_2 \tilde{f}_{ng_{ox}} + q_3 \tilde{f}_{ng_{oy}} + q_4 \tilde{f}_{ng_{oz}} & -q_1 \tilde{f}_{ng_{ox}} - q_4 \tilde{f}_{ng_{oy}} + q_3 \tilde{f}_{ng_{oz}} & \\ q_1 \tilde{f}_{ng_{ox}} + q_4 \tilde{f}_{ng_{oy}} - q_3 \tilde{f}_{ng_{oz}} & q_2 \tilde{f}_{ng_{ox}} + q_3 \tilde{f}_{ng_{oy}} + q_4 \tilde{f}_{ng_{oz}} & & \end{bmatrix}. \end{aligned} \quad (19)$$

The matrix Ψ is used to relate the current-time quaternion rate to the attitude rate vector ω :

$$\Psi = \frac{\partial \dot{\mathbf{q}}}{\partial \omega} = \frac{1}{2} \begin{bmatrix} -q_2 & -q_3 & -q_4 \\ q_1 & -q_4 & q_3 \\ q_4 & q_1 & -q_2 \\ -q_3 & q_2 & q_1 \end{bmatrix} \quad (20)$$

Finally, the partial derivatives of the inertial measurements, that is, the gyro attitude rate measurements and the accelerometer sensed non-gravitational forces, are given. The gyro measurement partials are easily determined, as they are functions of only the attitude rate states:

$$\frac{\partial \omega_x}{\partial \omega_x} = \frac{\partial \omega_y}{\partial \omega_y} = \frac{\partial \omega_z}{\partial \omega_z} = 1.0 \quad (21)$$

The accelerometer measurement partials are also straightforward to express, and are given here:

$$\frac{\partial a_x}{\partial f_{ng_x}} = \frac{\partial a_y}{\partial f_{ng_y}} = \frac{\partial a_z}{\partial f_{ng_z}} = 1.0 \quad (22)$$

$$\begin{aligned} \frac{\partial a_x}{\partial \omega_x} &= \omega_y r_{a_y} + \omega_z r_{a_z} & \frac{\partial a_x}{\partial \alpha_x} &= 0 \\ \frac{\partial a_x}{\partial \omega_y} &= -2\omega_y r_{a_x} + \omega_x r_{a_y} & \frac{\partial a_x}{\partial \alpha_y} &= r_{a_z} \\ \frac{\partial a_x}{\partial \omega_z} &= -2\omega_z r_{a_x} + \omega_x r_{a_z} & \frac{\partial a_x}{\partial \alpha_z} &= -r_{a_y} \end{aligned} \quad (23)$$

$$\begin{aligned} \frac{\partial a_y}{\partial \omega_x} &= \omega_y r_{a_x} - 2\omega_x r_{a_y} & \frac{\partial a_y}{\partial \alpha_x} &= -r_{a_z} \\ \frac{\partial a_y}{\partial \omega_y} &= \omega_x r_{a_x} + \omega_z r_{a_z} & \frac{\partial a_y}{\partial \alpha_y} &= 0 \\ \frac{\partial a_y}{\partial \omega_z} &= -2\omega_z r_{a_y} + \omega_y r_{a_z} & \frac{\partial a_y}{\partial \alpha_z} &= r_{a_x} \end{aligned} \quad (24)$$

$$\begin{aligned}
\frac{\partial a_z}{\partial \omega_x} &= \omega_z r_{a_x} - 2\omega_x r_{a_z} & \frac{\partial a_z}{\partial \alpha_x} &= r_{a_y} \\
\frac{\partial a_z}{\partial \omega_y} &= \omega_z r_{a_y} - 2\omega_y r_{a_z} & \frac{\partial a_z}{\partial \alpha_y} &= -r_{a_x} \\
\frac{\partial a_z}{\partial \omega_z} &= \omega_x r_{a_x} + \omega_y r_{a_y} & \frac{\partial a_z}{\partial \alpha_z} &= 0
\end{aligned} \tag{25}$$

As explained above, REDLand is an extended Kalman filter (EKF), a well-known recursive estimation approach. Since the formulation of the EKF is discussed widely in the literature, the authors will not repeat the algorithm here.^{1,4} Instead, this paper focuses on the discussion of the REDLand equations of motion, and treatment of inertial measurements. Nonetheless, the one characteristic of this filter that must be mentioned is that the process noise is increased when rapid changes of acceleration are observed, hopefully accounting for any unmodeled events.

RESULTS

During the months of September and October of 2001, the first series of drop tests using the new MER drop test lander were conducted at the SPF. Eight different drops were conducted. The first seven drops were “down-bag/edge” drops, that is, one lander face’s normal was directed at the ground and one edge was perpendicular to the ramp surface’s normal (see Figure 7). The final drop was an “up-bag/edge” drop, one lander face’s normal was directed towards the ceiling. This paper will use the data from the final drop to illustrate the results from the REDLand filter.

To start, Figure 8 is taken from a three-dimensional movie created in MATLAB from the position and attitude data, rotated into the Mars frame. The frame rate is 20 Hz. The “Roll Line” is the would-be path of the center of mass in a perfectly inelastic collision with the ramp.

Knowledge of the acceleration environment has proven useful to structural engineers. In this drop, the MER drop test lander was instrumented with four accelerometers on the base petal (BP, PYBP, PXBP, and MXBP from Figure 5). Knowledge of the locations of these accelerometers relative to a reference point enables REDLand to estimate that acceleration environment. Knowing the attitude of the lander allows for a rotation from body coordinates to Mars frame coordinates. Figure 9 shows these two views of the non-gravitational translational acceleration. Since the the Z-axis in the body and SPF frames were parallel for this drop before impact, the accelerating effect of the bungee is noticeable. Figure 10 shows the rotational velocity and acceleration. The use of a rate gyroscope, as in this case, assists in determining the rotational velocity.

The last of the estimated rotational state is the quaternion. As a representation of attitude, the quaternion is difficult to visualize. However, with the correct mapping, it is simple to estimate. Figure 11 shows the estimated quaternion (from the lab to body reference frames) and the corresponding aerospace (1-2-3) Euler angles for reference.

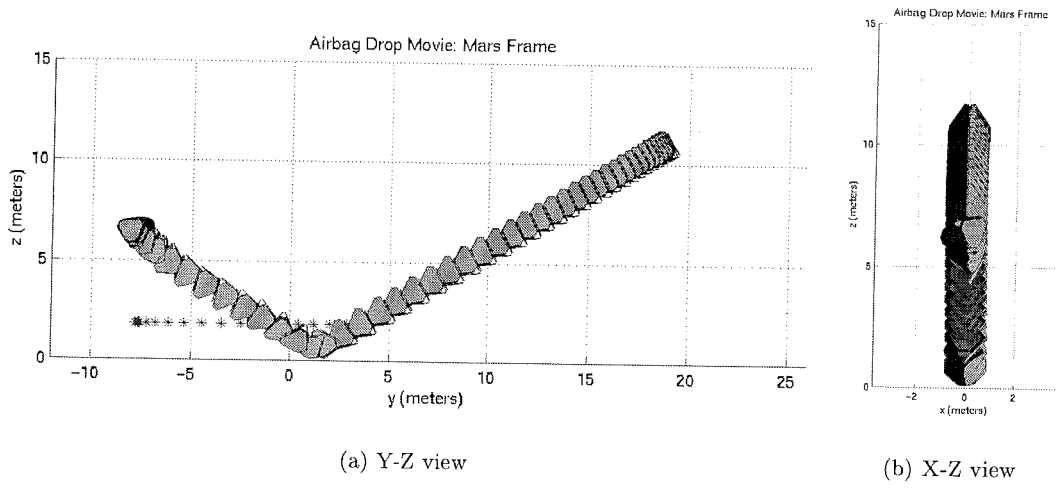


Figure 8: Reconstructed trajectory in the Mars Frame

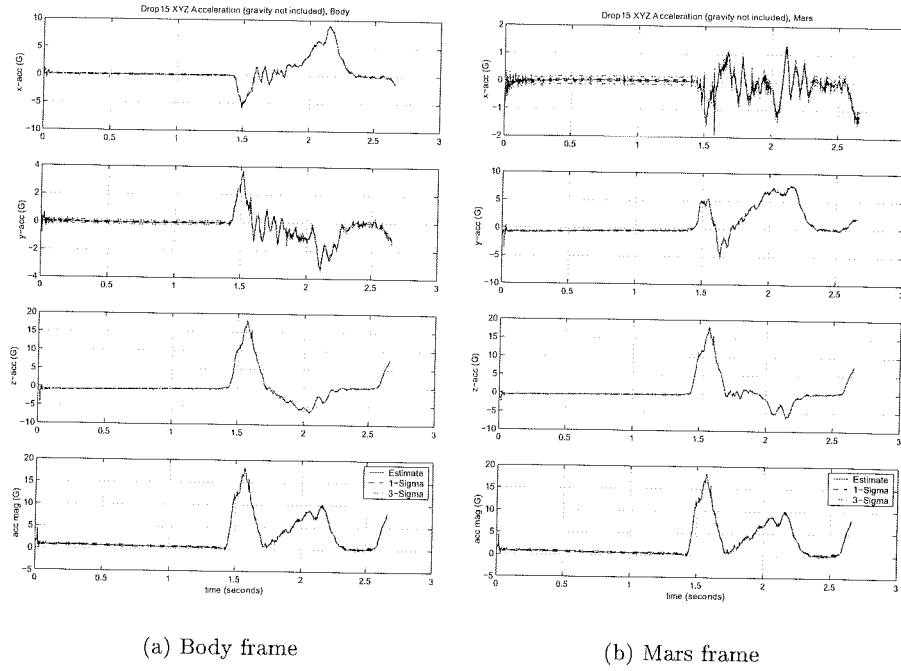


Figure 9: Translational acceleration of the lander's center of mass (\mathbf{f}_{ng_o}) verse time.

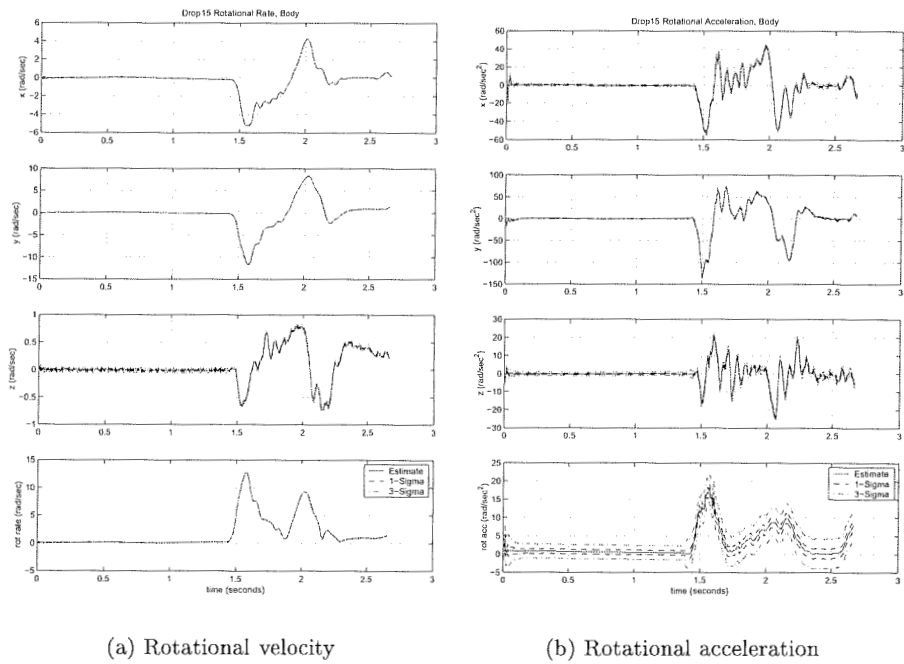


Figure 10: Rotational velocity (ω) and acceleration (α) of the lander verse time.

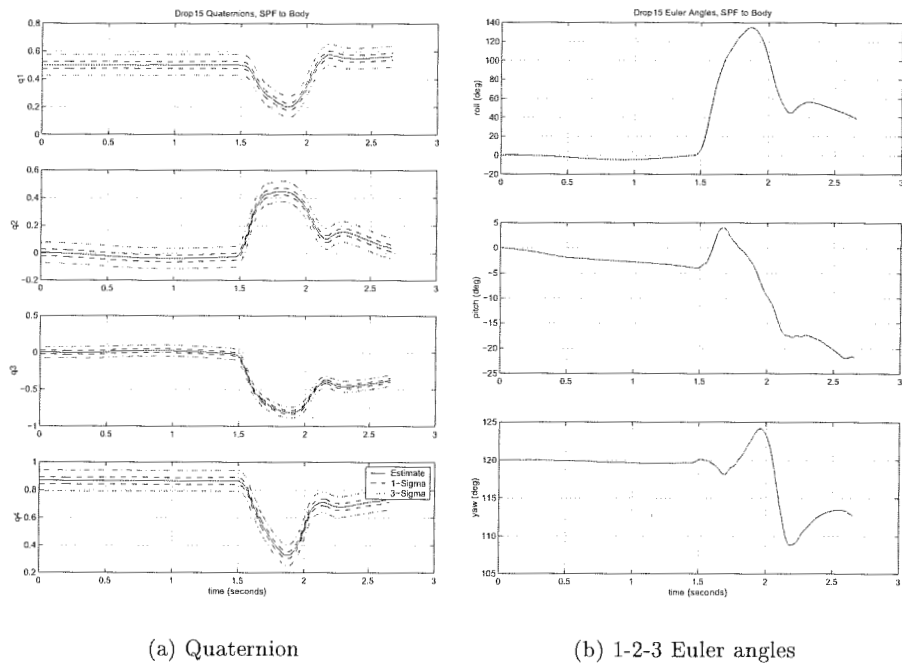
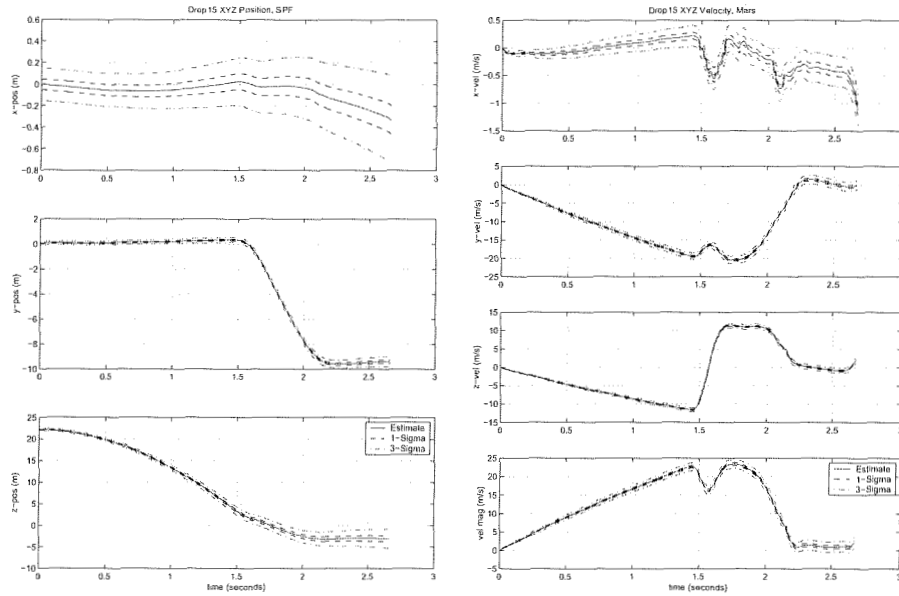


Figure 11: Quaternion and Euler angle representations of the SPF to body attitude.



(a) Position in the SPF frame

(b) Velocity in the Mars frame

Figure 12: Position ($\tilde{\mathbf{r}}_o$) and velocity ($\tilde{\mathbf{v}}_o$) estimates verse time.

The final states of interest, position and velocity, are estimated and shown as functions of time in Figure 12. The estimates of the position and velocity of the lander’s center of mass is based on the initial conditions of the hanging lander before the release (the importance of which will be discussed in the next section), the translational acceleration, and the attitude. Worth mentioning is that one can quantify a coefficient of restitution for the airbags based on the ratio of velocity after the impact to the velocity before the impact in the surface normal direction (+Z in the Mars frame).

Finally, a characterization of airbag stroke can be taken from the position and attitude information. Figure 13 shows the distance from the surface to the closest point on the lander at that instant and the 1σ uncertainty of that measurement. The point of closest approach is the maximum stroke event.

ERROR SOURCES

As seen in the figures of the preceding section, estimating the states for which measurements are made yields results with low uncertainties. The accelerometers are accurate to 0.2 G and the rate gyroscope is accurate to 0.4 degrees. As the estimator moves up the anti-derivative chain, the uncertainties of the estimated, unmeasured states grow with time. The rate of the growth of these states is related to the value of their derivative’s uncertainties. For example, the uncertainty of the quaternion grows very little over the three-second time frame because the uncertainty of the rotational rate is both small and

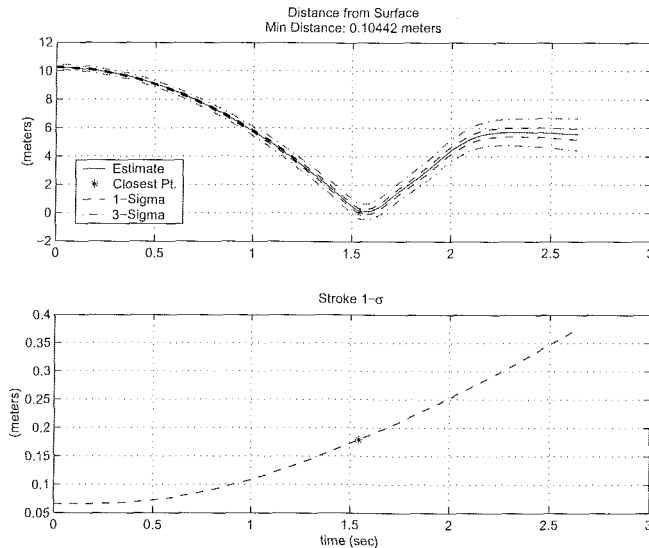


Figure 13: The top plot shows the distance from the ramp surface to the closest point on the lander. The bottom plot shows the $1 - \sigma$ uncertainty of that estimate.

nearly constant. However, the uncertainty of the translational acceleration is large enough to noticeably grow the uncertainty of the translational velocity, which, in turn, grows the the uncertainty of the position rapidly. Figure 14 illustrates the 1σ uncertainties of all states as functions of time.

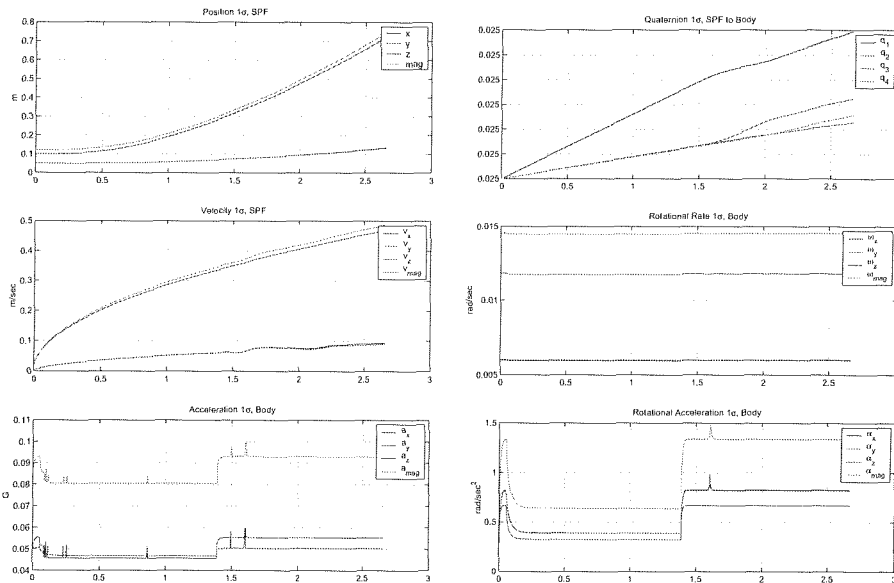
Another significant error source is the *a priori* attitude. Since rotational rate and acceleration are measured, the quaternion as a function of time is based on the its *a priori* value and the change throughout the run. The *a priori* quaternion is determined by visual inspection or by a three-axis accelerometer and magnetometer measuring device (MicroStrain's 3DM). The largest error source of the former is human judgement, since the inspection takes place via video monitors in a control room. The largest error source of the latter is from the measurement uncertainty of the gravity and magnetic field vectors. For this trial, raw measurements from the 3DM were used to construct two vectors, from which a rotation matrix, then a quaternion can be formed. The *a priori* covariance of the quaternion is mapped from these vectors (\mathbf{u} and \mathbf{v}) via the following transform:

$$\mathbf{P}_{\mathbf{q},4 \times 4} = \mathbf{D}_{4 \times 6} \mathbf{P}_{\mathbf{u},\mathbf{v},6 \times 6} \mathbf{D}_{6 \times 4}^T \quad (26)$$

where

$$\mathbf{D}_{4 \times 6} = \frac{\partial \mathbf{q}}{\partial (\mathbf{u}, \mathbf{v})}. \quad (27)$$

One way to reduce the growth of all uncertainties is to have range measurements. These would not only reduce the uncertainties of all the states, it would also lead to a more truer estimate of those states. Figures 8 and 13 show the lander nearly going through the



(a) Translational

(b) Rotational

Figure 14: Translational and rotational 1σ uncertainties as functions of time

ramp surface. Video of the drop suggests that the lander may not be this close to full-stroke. If the initial conditions are changed by a small amount, the estimate may show the lander going through the ramp. However, that phenomenon is not observed.

These results are based on inexact *a priori* knowledge of the position and velocity at the start of the drop. Without new measurements in this kinematic environment, the *a priori* uncertainties for the unmeasured states are smallest uncertainties for those states throughout the drop. During the next series of drop tests, an odometer will be attached to a sheave in the bungee acceleration system, from which range measurements can be made to the lander during the drop. Radar guns in the SPF may also provide additional measurements.

CONCLUSIONS AND FUTURE WORK

The REDLand filter software described in this paper is largely tailored to working with data collected from the MER airbag drop tests. In its current state, it yields accurate results on the acceleration environment of the lander. However, the results of the other states are only as good as their *a priori* uncertainties. With added measurements, such as range and velocity, the knowledge of the airbag stroke will be greatly improved.

The reconstruction of the airbag impact stroke events using REDLand is planned to continue in conjunction with the regime of tests being carried out for MER. No future plans exist for continued use of the REDLand software itself beyond the MER airbag drop

tests. However, the REDLand inertial measurement processing algorithms are serving to inform the design of software being developed at JPL to reconstruct 6-degree-of-freedom trajectories of space vehicles that perform aeroassist maneuvers, that is, maneuvers such as aerobraking, aerocapture, or EDL.

ACKNOWLEDGEMENTS

The authors would like to thank Joe Guinn, Ralph Roncolli, Phil Knocke, Wayne Lee, Adam Steltzner, Tom Rivellini, Greg Davis, Stacy Weinstein, John Carson, Doug Adams, Ed Konefat, Tony Zavala, and Gary Bruner at JPL, Skip Wilson, Jim Stein, and the rest of the ILC Dover airbag test and design teams, the SPF team at NASA Glenn Research Center at Plum Brook Station, and Jim Blaker of Robert A. Denton, Inc. (ret.).

This research was carried out at the Jet Propulsion Laboratory, California Institute of Technology, under a contract with the National Aeronautics and Space Administration.

Reference herein to any specific commercial product, process, or service by trade name, trademark, manufacturer, or otherwise, does not constitute or imply its endorsement by the United States Government or the Jet Propulsion Laboratory, California Institute of Technology.

REFERENCES

- [1] Bierman, G.J., *Factorization Methods for Discrete Sequential Estimation*, Academic Press, New York, 1977.
- [2] Cadogan, D., C. Sandy, M Grahne, "Development and Evaluation of the Mars Pathfinder Inflatable Airbag Landing System", 49th International Astronautical Congress, Melbourne, Australia, September 28, 1998.
- [3] Davis, Gregory L., "The Results of Dynamic Data Acquisition During Mars Pathfinder Prototype Airbag Drop Testing" Proceedings of the 67th Shock and Vibration Symposium, Volume I, Monterey, CA, November 1996, pp. 197-208.
- [4] Gelb, A., ed., *Applied Optimal Estimation*, MIT Press, Cambridge, MA, 1974.
- [5] "MER Development Model 3 Airbag Drop Test Plan," ILC Dover, Inc., Frederica, DE, September 2001.
- [6] "World Class Facilities CD-ROM", NASA Glenn Research Center at Lewis Field Productions, Cleveland, OH, 2000.
- [7] Rivellini, Tommaso P., "Development Testing of the Mars Pathfinder Inflatable Landing System", Engineering, Construction and Operations in Space 5, Proceedings of 5th International Conference on Space '96, Volume II, published by American Society of Civil Engineers, New York, NY, 1996, pp. 1059-1068.
- [8] Wertz, James R., *Spacecraft Attitude Determination and Control*, D. Reidel, Dordrecht, Holland, 1978, pp. 410-428.